SUPPLEMENTAL APPENDIX

SUPPLEMENTAL METHODS

Animal phenotyping

All animals in this study were male Sprague Dawley rats (Charles River, Germany), weighing at the start of the experiment 180-200gr. At the beginning of the study rats were randomly allocated into two groups: controls (ConNx, N=15) and the ones receiving Su5416, followed by hypoxia (N=28). 1-week post-hypoxia 11 randomly picked animals from the second group received TPHi orally (SuHx + TPHi), and 17 animals remained untreated (SuHx).

Cardiac catheterization (closed chest technique). Cardiac catheterization was performed as described previously(1). Measurements of the right side parameters (RV systolic pressure (RVSP), RV end-diastolic pressure (RVEDP) and RV dp/dt max. and min.) were followed in the same animal by measuring systemic parameters (systolic (SBP), diastolic (DBP)) as well as the left side parameter (LV end-diastolic pressure (LVEDP)). All measurements were performed under isoflurane anesthesia (2.0-3.0% isoflurane, 100% oxygen 2 L/min) in spontaneously breathing animals.

Echocardiography was performed as described previously(1). Measurements of heart rate, ventricular dimensions and function, and PA pressure surrogates were conducted in spontaneously breathing animals under isoflurane anesthesia using an ultrasound machine (Vevo 2100 System, VisualSonics Inc.) equipped with a 17 MHz linear array transducer.

Analysis of tissue (ex vivo)

Tissue perfusion, harvest, and preparation for RNA analysis. In deep isoflurane anesthesia (5%), the abdominal aorta of rats was dissected, and the animal was allowed to bleed out. The rat lungs were perfused *in situ* by injecting 60 ml of normal saline into the RV. After perfusion,

heart and lungs were taken out "en bloc;" the left lung lobe was ligated and snap-frozen in liquid nitrogen, while the right lobes were tracheally inflated with 10% formalin, fixed at +4°C, and then embedded in paraffin for standard histology. In parallel, the heart was separated and placed in ice-cold cardioplegic solution (0.5M KCl in 0.9% NaCl) for 1 minute. Afterwards the heart was briefly rinsed in PBS and dissected: a subset of hearts (RV, LV) was snap-frozen in liquid nitrogen and then transferred to -80°C for the subsequent RNA analysis while another subset of hearts was fixed in buffered formalin +4°C, and then embedded in paraffin for further histological assessment.

Tissue preparation for RNA sequencing. The collected tissue subjected to further RNA extraction was pre-treated with RNAlater-ICE Frozen Tissue Transition Solution (Ambion) and stored at -20°C. Approximately 50 mg of tissue were homogenized in TRIzol and used for total RNA extraction according to the manufacturer's protocol (TRIzol, Life Technologies).

Histology

Hematoxylin and eosin (H&E) and Masson's Trichrome stainings were performed according to standard protocols.

To determine the perivascular collagen deposition of medium-to-small (<100 μm) vessels, a percentage of the collagen-positive area (blue) over the perivascular area of the vessel was calculated in the sections stained for Masson's Trichrome. The collagen deposition was assessed .in a minimum of 20 vessels per animal at 200x magnification.

To determine muscularization of small (<50 μm) peripheral pulmonary arteries, 3 μm tissue sections were incubated with primary antibodies against α-smooth muscle actin (α-SMA, A2547, 1:125, Sigma) overnight, further incubated with Peroxidase AffiniPure Donkey Anti-Mouse IgG (H+L) (715-035-151, 1:1000, Jackson ImmunoResearch Europe LTD), visualized with ImmPACT DAB solution (Vector Laboratories), and counterstained with hematoxylin

solution, Harris modified. Pulmonary vessel wall thickness was assessed by measuring α-SMA positive staining in a minimum of 20 vessels (<50 μm diameter) per animal at 200x magnification. The wall thickness was determined as media thickness index using ImageJ software and compared between the groups, where media thickness index

is $\frac{area_{ext}-area_{int}}{area_{ext}}$, $area_{ext}$ and $area_{int}$ being the areas within the external and internal boundaries of the α-SMA layer, respectively.

For immunofluorescence lung paraffin sections were deparaffinized, rehydrated and unmasked using 0.1 mM TRIS-EDTA buffer containing 0.01% Tween-20, at pH 9. They were incubated with the primary antibodies in a wet chamber at 4°C overnight before incubating with secondary antibodies. Finally, the cover slips were mounted using Fluoromount-G with DAPI (BIOZOL). Images were taken using an inverted light-fluorescence Keyence microscope (Japan). The analysis and quantification were done using the Keyence analyzer BZ-X800 (Japan).

Antibodies used:

Following different primary antibodies (AB) were used in the present study (all from Proteintech, Germany): PCNA rabbit polyclonal AB (#24036-1-AP, 1:500), CD3 rabbit polyclonal AB (cat. #17617-1-AP, 1:500), F4/80 rabbit polyclonal AB (cat. #28463-1-AP, 1:500), and CD68 rabbit polyclonal AB (cat. #28058-1-AP, 1:500). The secondary donkey anti-rabbit antibody conjugated with Cy3 (Jackson Lab., cat. #711-165-152) was used in concentration of 1:500 for all primary antibodies.

For all target proteins in immunofluorescent pictures (Figure 4), 5-10 microscopic images from each lung lobe present on the slide were taken and the nucleated cells were counted (had DAPI+Cy3 signal).

RNA sequencing

RNA-sequencing was performed by BGI (Shanghai, China). TruSeq® transcriptome libraries were prepared following established protocols from Illumina and mRNA was sequenced using the DNBseq platform (150 bp paired-end reads). The sequencing reads were aligned to the rat genome (Rnor_6.0.96) using STAR (2) and the read counts corresponding to the Ensembl-annotated genes were quantified using RSEM (3). Differential expression analysis was performed using DESeq2 (4) after within-lane GC normalization by EDASeq (5). Benjamini-Hochberg false discovery rate (FDR) procedure was applied to correct for multiple testing. Differentially expressed genes (DEGs) with FDR-adjusted P values < 0.05 and fold changes > 2 or < 0.5 were considered significantly differentially expressed.

Drug discovery and synthesis

For the complete description of drug discovery, please refer to (6).

Initially, we screened the FMP library (7) containing 37.000 compounds and focused on a small hit cluster of 3 compounds consisting of a xanthine core. One structure of the hit cluster is shown in **Supplemental Figure 1**. Due to its structural similarity to the co-substrate pterin (BH_4) we selected the xanthine scaffold for further optimization. Based on structure-based drug design (SBDD) we extended the alkyl chain attached to N^3 and shortened the alkyl chain at N^7 in order to increase the inhibitory potency of the hit series. Furthermore, we developed a novel synthesis in 10 steps to exchange the sulfur atom against a carbon atom between the xanthine core and the benzimidazole ring as well as attached a dioxolane ring to the benzimidazole ring. Both modifications boosted the overall oxidative stability of TPT-001. Finally, this lead optimization resulted in a class of xanthine derivatives with IC_{50} in the nanomolar range. The optimized inhibitor TPT-001 covers simultaneously the co-substrate pterin and the tryptophan binding sites of the TPH1 binding pocket together with a strong chelation to the catalytically active iron cation. This unexpected binding mode makes the novel inhibitor less susceptible for

physiological alterations of tryptophan levels and reduces the risk of possible off-target effects. The inhibitor series can be found in the protein database (https://www.rcsb.org/) bound to the human TPH1 using the following codes 7ZIF, 7ZIH, 7ZIJ, 7ZIG, 7ZII, and 7ZIK. The crystal structure 7ZII contains an inhibitor which is structurally very similar to the described inhibitor herein (n-propyl versus an ethyl side chain attached to N^3 of the xanthine core). 7ZIK comprises the binding mode of telotristat which is structurally similar to TPH inhibitor rodatristat (KAR5585).

SUPPLEMENTAL DISCUSSION

The idea that inhibiting serotonin pathway could be beneficial for treatment of PAH derives from observation in the 1990s, when weight loss drugs were found to be causal of the disease. It was shown that drugs like aminoxaphen induce serotonin release via serotonin transporter SERT (8). Additionally, these drugs can be metabolized in the body into a 5-HT2 receptor agonists (norfenfluramine) (9). Dexfenfluramine was shown to induce PAH and pulmonary-vascular remodeling in the presence of peripheral serotonin only, and both overexpression of SERT and dexfenfluramine supplementation had additive effects on vascular remodeling (10).

A number of studies related to serotonin pathways have been performed on cells from the pulmonary vasculature. PASMCs isolated from a female PAH patient showed an abundant expression of 5-HT1B receptor (11). The serotonin transporter SERT and 5-HT1B together induce PASMC proliferation and contraction (12). In PASMCs, serotonin receptor-mediated signaling activates vasoconstrictive Ca2+ pathways and in turn stimulates expression of proliferative and profibrotic genes (13). These effects are mediated by several serotonin receptors, including 5-HT2A and 5-HT1B (14).

It has also been shown that overexpression of SERT in pulmonary arteries is causal for PAH (15,16). SERT increases the cytosolic concentration of serotonin and thereby serotonylation, a posttranslational modification (17,18), that may play an important role in the development of pathological signatures in cells. Rho kinase, when serotonylated at the glutamine residue, causes constriction in cells (19). It has also been speculated that serotonylated fibronectin regulates smooth muscle cell proliferation and migration, however the exact mechanism remains unknown (20).

Supplemental Figure 1

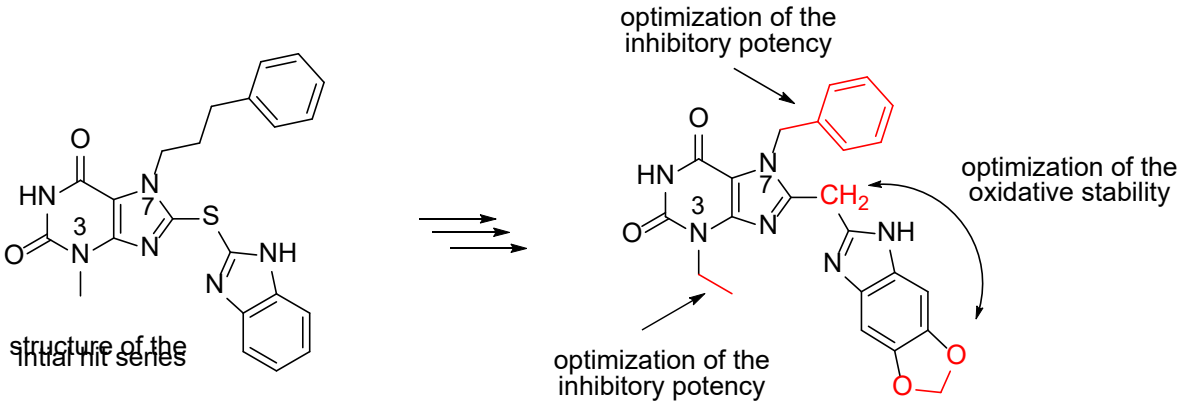

Supplemental Figure 1. Optimization of tryptophan hydroxylase inhibitor TPT-001

SUPPLEMENTAL REFERENCES

1. Legchenko E, Chouvarine P, Borchert P et al. The PPARgamma agonist pioglitazone reverses pulmonary hypertension and prevents right heart failure via fatty acid oxidation. Sci Transl Med 2018;10:eaao0303
2. Dobin A, Davis CA, Schlesinger F et al. STAR: ultrafast universal RNA-seq aligner. Bioinformatics 2013;29:15-21.
3. Li B, Dewey CN. RSEM: accurate transcript quantification from RNA-Seq data with or without a reference genome. BMC Bioinformatics 2011;12:323.
4. Love MI, Huber W, Anders S. Moderated estimation of fold change and dispersion for RNA-seq data with DESeq2. Genome Biol 2014;15:550.
5. Risso D, Schwartz K, Sherlock G, Dudoit S. GC-content normalization for RNA-Seq data. BMC Bioinformatics 2011;12:480.
6. Specker E, Matthes S, Wesolowski R et al. Structure-based design of xanthine-benzimidazole derivatives as novel and potent tryptophan hydroxylase inhibitors. J Med Chem 2022;65:11126-11149.
7. Lisurek M, Rupp B, Wichard J et al. Design of chemical libraries with potentially bioactive molecules applying a maximum common substructure concept. Mol Divers 2010;14:401-8.
8. Rothman RB, Ayestas MA, Dersch CM, Baumann MH. Aminorex, fenfluramine, and chlorphentermine are serotonin transporter substrates. Implications for primary pulmonary hypertension. Circulation 1999;100:869-75.
9. Fitzgerald LW, Burn TC, Brown BS et al. Possible role of valvular serotonin 5-HT(2B) receptors in the cardiopathy associated with fenfluramine. Mol Pharmacol 2000;57:75-81.

10. Dempsie Y, Morecroft I, Welsh DJ et al. Converging evidence in support of the serotonin hypothesis of dexfenfluramine-induced pulmonary hypertension with novel transgenic mice. Circulation 2008;117:2928-37.

11. Wallace E, Morrell NW, Yang XD et al. A sex-specific microRNA-96/5-hydroxytryptamine 1B axis influences development of pulmonary hypertension. Am J Respir Crit Care Med 2015;191:1432-42.

12. MacLean MMR. The serotonin hypothesis in pulmonary hypertension revisited: targets for novel therapies (2017 Grover Conference Series). Pulm Circ 2018;8:2045894018759125.

13. Cogolludo A, Moreno L, Lodi F et al. Serotonin inhibits voltage-gated K^+ currents in pulmonary artery smooth muscle cells: role of 5-HT2A receptors, caveolin-1, and KV1.5 channel internalization. Circ Res 2006;98:931-8.

14. MacLean MR, Fanburg B, Hill N et al. Serotonin and pulmonary hypertension; sex and drugs and ROCK and rho. Compr Physiol 2022;12:4103-4118.

15. MacLean MR, Deuchar GA, Hicks MN et al. Overexpression of the 5-hydroxytryptamine transporter gene: effect on pulmonary hemodynamics and hypoxia-induced pulmonary hypertension. Circulation 2004;109:2150-5.

16. Guignabert C, Izikki M, Tu LI et al. Transgenic mice overexpressing the 5-hydroxytryptamine transporter gene in smooth muscle develop pulmonary hypertension. Circ Res 2006;98:1323-30.

17. Walther DJ, Peter JU, Bashammakh S et al. Synthesis of serotonin by a second tryptophan hydroxylase isoform. Science 2003;299:76.

18. Bader M. Serotonylation: serotonin signaling and epigenetics. Front Mol Neurosci 2019;12:288.

19. Liu Y, Wei L, Laskin DL, Fanburg BL. Role of protein transamidation in serotonin-induced proliferation and migration of pulmonary artery smooth muscle cells. Am J Respir Cell Mol Biol 2011;44:548-55.

20. Wei L, Warburton RR, Preston IR et al. Serotonylated fibronectin is elevated in pulmonary hypertension. Am J Physiol Lung Cell Mol Physiol 2012;302:L1273-9.